Tuning Optical Properties of Dibenzochrysenes by Functionalization: A Many-Body Perturbation Theory Study

Nicolas Dardenne,[†] Roberto Cardia,[‡,§] Jing Li,[∥] Giuliano Malloci,[‡] Giancarlo Cappellini,[‡,§] Xavier Blase,[∥] Jean-Christophe Charlier,[†] and Gian-Marco Rignanese*,[†]

[†]Institute of Condensed Matter and Nanoscience (IMCN), Université catholique de Louvain, B-1348 Louvain-la-Neuve, Belgium
[‡]Università degli Studi di Cagliari, Dipartimento di Fisica, Cittadella Universitaria, I-09042 Monserrato, Cagliari, Italy
[§]Istituto Officina dei Materiali (CNR - IOM), UOS di Cagliari, Cittadella Universitaria, I-09042 Monserrato, Cagliari, Italy
[∥]CNRS and Grenoble-Alpes University, Institut Néel, F-38042 Grenoble, France

ABSTRACT: Using many-body perturbation theory, the optical properties of modified compact and angular dibenzochrysenes are investigated. First, for a series of already existing molecules in that family, the computed absorption spectra are benchmarked against experimental data in order to evaluate the strengths and the limitations of the method. Then, the computed absorption spectra are presented for newly designed dibenzochrysenes. One of the main results is that the addition of thiophenyl groups at specific positions produces an enhancement of the absorption in the visible region. The information provided in this study can be used as a guide to synthesize optimized materials for solar cells.
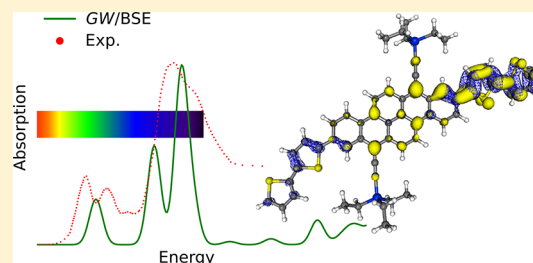
INTRODUCTION

Small polycyclic aromatic hydrocarbons (PAHs) are being intensively studied due to their applications in different optoelectronic devices such as organic field effect transistors (OFETs), organic light-emitting diodes (OLEDs), and organic photovoltaic (OPV) cells.[1−6] Compared to conjugated polymers, these soft organic semiconductors offer several advantages such as the possibility to be easily purified by various techniques, to have accurate molecular weight control, and to be tractable by both evaporation and solution-processing methods.[7−10] Bulk heterojunction organic solar cells built with small-molecule dibenzochrysene as active donor material show good power conversion efficiencies. The angular dibenzo[b,def]chrysene and the compact dibenzo[def,mno]chrysene (A-DBC and C-DBC) present efficiencies of 2.2% and 1.95%, respectively, due to a high open-circuit voltage related to their low-lying HOMO levels.[11,12] These molecules also exhibit good chemical stability. Also, with their π-conjugated backbone, they can assemble in a well packed structure due the strong π−π interactions. Moreover, their electronic, optical, and transport properties can be tuned via functionalization of the conjugated core.[13−16] Chemical modification of PAHs has already been tested in previous experimental[12,17−21] and theoretical[21,22] investigations but with only a few functional groups at a time.

The goal of this study is to present a systematic theoretical study of various functional groups tested in previous experimental works along with an analysis of a few newly designed materials. Many-body perturbation theory (MBPT) within the GW and Bethe−Salpeter equation (BSE) formalisms[23] is used to predict the absorption spectra of PAHs. First, the computational method is validated on a test set consisting of various PAHs. The computed absorption peaks are found to be in good agreement with the experimental ones. In addition, slight modifications due to the substitution of functional groups are correctly captured by the GW/BSE formalism. Then, newly designed PAHs are investigated. Starting from the A-DBC and C-DBC, various functional groups are attached to the molecules and their computed absorption spectra are analyzed focusing on their influence on the optical properties of DBCs. In particular, the addition of several thiophenyl groups on a DBC is shown to shift the main absorption peaks down from high energies to the visible region. The discovered trends can be used as guidelines to design optimized materials for harvesting the solar energy.

METHOD

For all the molecules considered, the atomic positions are first fully relaxed within density functional theory (DFT)[24,25] using the NWChem package.[26] The Becke three-parameter Lee−Yang−Parr (B3LYP) hybrid exchange-correlation functional[27,28] is adopted in combination with the Pople 6-31G basis set.[29] The size of the basis set was tested by comparing the optimized geometries obtained with the larger 6-31+G* basis set for a few molecules. The bond lengths were found to vary by less than 0.01 Å for the first and second row atoms and 0.2 Å for the few third row atoms. The resulting electronic properties of the compounds were found to be very similar. As far as the exchange-correlation functional is concerned, the effect of adding an empirical dispersion correction term[30] to the B3LYP functional has already
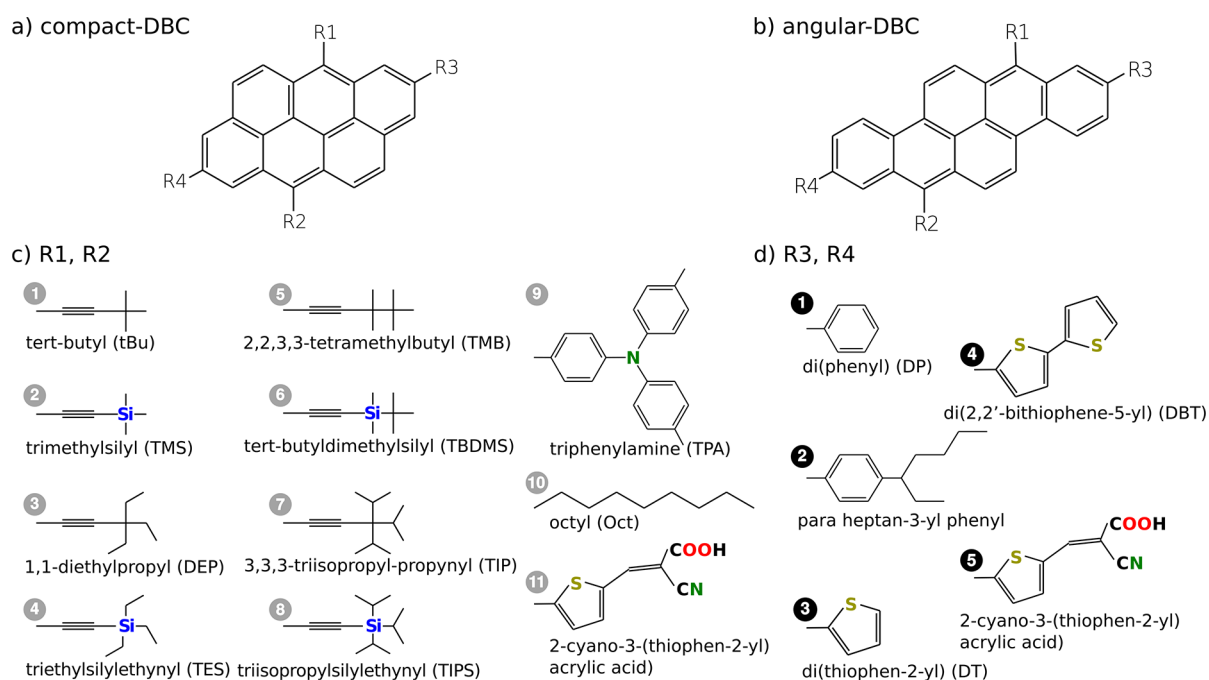
Figure 1. Illustration of the compact (a) and angular (b) dibenzochrysenes. Various functional groups with their nomenclature attached at R1 and R2 positions (c) and at R3 and R4 positions (d).
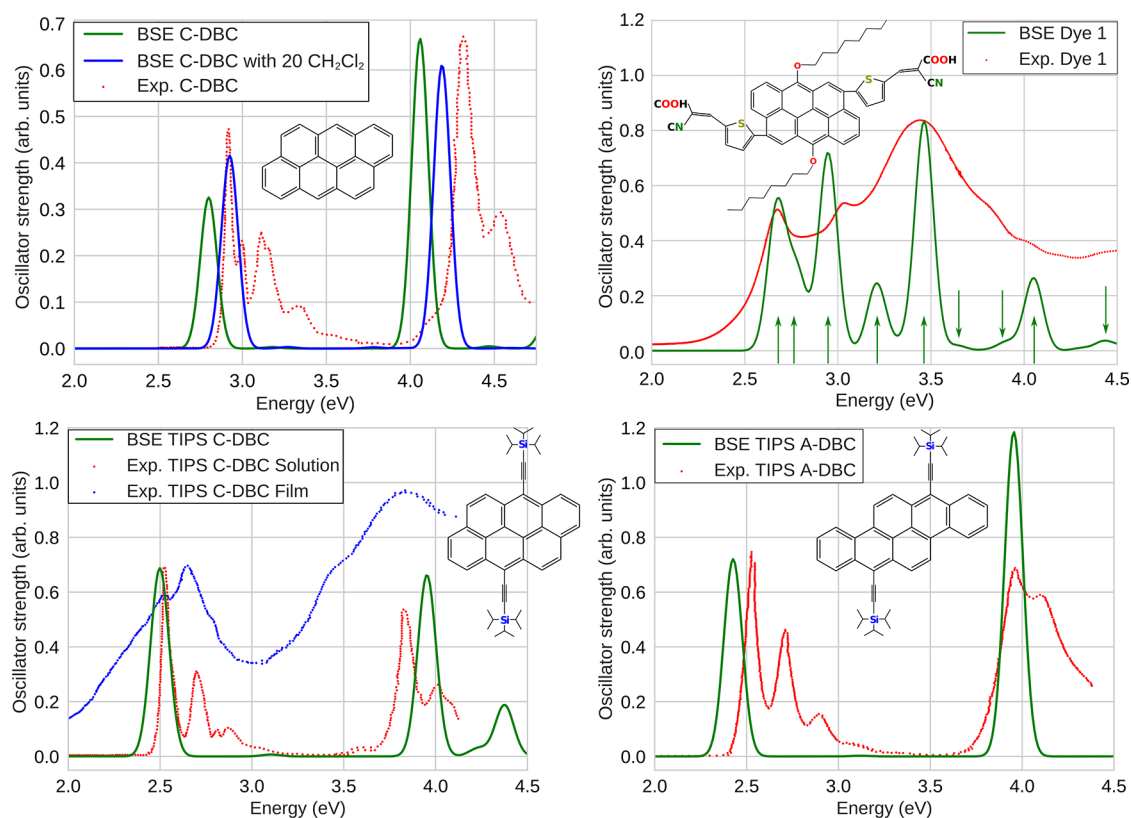
Figure 2. Comparison between experimental (red) and computed (green) absorption spectra for the C-DBC (upper left), Dye 1 (upper right), TIPS-C-DBC (lower left, C-R1R2-8), and TIPS-A-DBC (lower right, A-R1R2-8). The experimental spectra are from refs 40, 19, 12, and 17, respectively. In the upper left graph, the absorption spectrum for C-DBC with a first solvation shell of CH_2Cl_2 is plotted in blue. In the lower left graph, the absorption spectrum of a thin film TIPS-C-DBC is plotted in blue. In the upper right graph, the nine theoretical absorption peaks (1−9 from left to right) are indicated with green arrows.

been shown[22] to produce small differences in the geometries (root-mean-square displacement less than 1 Å) without significantly modifying the electronic properties.

Using the optimized geometries, GW/BSE calculations are performed with the FIESTA package.[31−33] The Green's function G and the screened Coulomb potential W are built from the

Table 1. Comparison between Experiment (in Solution with CH₂Cl₂) and Theory of HOMO/LUMO Levels and Optical Gaps for Various DBC Molecules[a]

group	HOMO			LUMO			optical gap	
	GW	*GW**	exptl	*GW*	*GW**	exptl	BSE	exptl
tBU-	−6.43	−5.40	−5.26	−1.37	−2.79	−2.87	2.53	2.39
TMS-	−6.58	−5.53	−5.24	−1.57	−2.94	−2.96	2.40	2.38
TES-	−6.57	−5.55	−5.35	−1.60	−2.94	−2.97	2.41	2.38
TBDMS-	−6.59	−5.56	−5.38	−1.61	−2.92	−3.03	2.41	2.35

[a]For the HOMO/LUMO levels, the table shows the computed *GW* results in the gas phase, the values corrected to take into account the polarization effect (*GW**), and the experimental data (taken to be the negative of the ionization potential and electronic affinity). For the optical gaps, the BSE results correspond to the first exciton peak and the experimental values are the UV/vis onsets. The experimental data are taken from ref 18. All DBCs are angular type with various groups (listed in column 1) attached to the R1 and R2 positions. All energies are in eV.

Kohn−Sham eigenstates generated by the NWChem package with the M06-2X exchange-correlation functional[34] and the maug-cc-pvtz basis set.[35] Following a recent benchmark study of the optical absorption energies of a large standard set of organic molecules,[33] partially self-consistent *GW* calculations were performed, namely, reinjecting self-consistently the corrected quasiparticle energies in the construction of the Green's function *G* and the screened Coulomb potential *W*. It has been shown that this procedure leads to an excellent agreement with the best theoretical estimates provided by high-level quantum chemistry techniques (mean-absolute error of the order of 0.2 eV).[33] As for the BSE calculations, they are performed mixing excitations and deexcitations, beyond the Tamm−Dancoff approximation. The BSE formalism has been shown to predict accurately charge-transfer excitations[32,36] and even cyanine-like transitions,[37] both known to be problematic for standard TD-DFT calculations, resulting in a robust scheme showing the same $O(N^4)$ computational scaling than TD-DFT. The calculations provide a discrete set of excitonic states with energy E_i and their corresponding oscillator strengths f_i. These values allow one to construct an absorption spectrum as a sum of Gaussian functions centered in E_i of height f_i. The full width at half-maximum for each Gaussian is constant and arbitrarily fixed. With this formalism, the optical gap is the first exciton that is active, i.e., with a nonzero oscillator strength. More details about the methodology can be found in refs 31−33. Exploiting the fact that the NWChem package also implements the SMD (solvation model density) polarized continuum model,[38] an estimate of the polarization effect can be obtained as the difference between the solvated and gas phase levels calculated by the ΔSCF technique.[39]

■ RESULTS AND DISCUSSION

The molecules that will be discussed in this work are illustrated in Figure 1. The two simplest molecules are the C-DBC and A-DBC, respectively (Figure 1a,b). Starting from these two building blocks, various functional groups can be attached to the four R positions, namely, R1, R2, R3, and R4. These functional groups were found in previous experimental works on DBC.[12,17−20,40] Figure 1c,d illustrates the functional groups that can be attached to R1 and R2 positions and to R3 and R4 positions, respectively. The notation X-Y-Z will be used to define a molecule where X is either A or C (for angular or compact), Y is either R1R2 or R3R4 for the attachment positions, and Z is the corresponding label of the functional group. A molecule named A-R1R2-4 will thus correspond to an angular DBC with the functional group 4 in Figure 1c attached at R1 and R2 positions, whereas the molecule named C-R3R4-2 will be a compact DBC with the group 2 in Figure 1d attached to R3 and R4 positions.

Benchmarking. The upper left panel in Figure 2 shows the comparison between the BSE calculated and experimental absorption spectra of C-DBC taken in solution with CH₂Cl₂.[40] The experimental spectrum has been scaled in intensity in such a way that the height of the highest peak matches that of the corresponding peak in the computed spectra. The computed absorption onset is at 2.83 eV (first peak), while the experimental one is at 2.92 eV (offset of 0.09 eV). The second important peak in the BSE spectrum is at 4.08 eV, while experimentally it is at 4.32 eV (offset of 0.24 eV). The computed spectrum also presents two extremely small peaks at 3.25 and 4.5 eV but failed to correctly predict the smaller experimental secondary peaks between 3.0 and 3.5 eV and one around 4.54 eV. These secondary peaks could be the vibronic progressions associated with each electronic transition (e.g., peaks at 3.2 and 3.4 eV for compact DBC might be vibronic peaks of the 0−0 transition at 2.94 eV) which are missing because the electron-vibration coupling is not taken into account by the MBPT. The energy shifts are probably related to the solvation effects since experiments are carried out in solution, while our computations are performed on isolated molecules, meaning in gas phase.[41] As found in refs 17 and 42, similar discrepancies also appear between gas phase calculations and solvated experiments when using time-dependent DFT computations. As a first exploration of solvation effects, the absorption spectrum of the same C-DBC has been computed with a first explicit solvation shell of 20 dichloromethane molecules[43] which is the solvent used in the experience. The spectrum is plotted in blue in the upper left panel of Figure 2. For the first peak, the offset of 0.09 eV between experimental and computed data disappears, and the offset of 0.24 eV is reduced to 0.13 eV for the second peak. This clearly indicates that the offsets are mainly due to the solvent effect. However, the computing time that would be needed to simulate all the systems with an explicit solvation shell is prohibitive. Hence, the rest of our *GW*/BSE calculations will only be performed in the gas phase.

The upper right panel of Figure 2 compares experimental (taken in solution with tetrahydrofuran) and BSE absorption spectra for one compact DBC called Dye 1 in ref 19. The first and second experimental peaks are computed within 0.001 and 0.09 eV, respectively. The high values in between them could be explained by the small second theoretical peak at 2.78 eV. The combination of the fourth, fifth, sixth, seventh, and eighth theoretical peaks form the third broad experimental peak centered about 3.45 eV. This experimental peak presents two small bumps at ~3.8 and ~4.0 eV which could be linked to the seventh and eighth theoretical peaks. The ninth theoretical peak at 4.43 eV also seems to correspond to an increase in the experimental absorption at the same energy.

The graphs in the lower panels of Figure 2 show the comparison between the BSE and experimental absorption spectra of TIPS compact and angular DBC (C- and A- R1R2-8, respectively) taken in solution with $CHCl_3$.[12,17] For both molecules, the computed onset is slightly red-shifted (0.02 eV for TIPS C-DBC and 0.09 eV for TIPS A-DBC) and the computed spectra are also missing vibronic secondary peaks. For the second BSE peaks, a blue shift occurs for the TIPS C-DBC, while it seems to perfectly match for the TIPS A-DBC. In the lower left panel of Figure 2, the experimental absorption spectrum of a thin film C-DBC (in blue) shows a more continuous profile with only two broad absorption peaks centered at 2.65 and 3.85 eV. As compared to the experimental solution phase, the position of the main absorption peaks is blue-shifted by 0.15 eV for the first peak and by only 0.02 eV for the second peak. This comparison shows that the position of the main peaks in the solution phase is a good indicator for predicting the absorption range in the solid state. There is, however, a broadening in the solid phase due to dispersion effects and the formation of occupied and unoccupied energy bands.

Table 1 compares the gas phase *GW* HOMO and LUMO energy levels and BSE optical gap with experimental data in solution for various DBCs. As expected, due to the lack of solvent polarization effects, the gas phase HOMO and LUMO *GW* energy levels are found to be larger and smaller, respectively, as compared to the reference values in solution. The solvent reaction field is known to stabilize added holes or electrons in a photoemission experiment in solution, with typical polarization energies of 1 eV or more.[44,45] The polarization energy induced by the dichloromethane has been estimated with the SMD model (with a 6-31+G* basis set and the B3LYP functional). By taking into account these solvent effects (*GW** in Table 1), the HOMO and LUMO levels are in better agreement with the experiments. On the other hand, the BSE optical gaps seem to correctly predict the vis/UV onset with an average and maximum error of 0.06 and 0.14 eV, respectively. The exciton, being a neutral excitation, is less sensitive to the surrounding dielectric medium and the absence of the solvent is less detrimental.

As a last benchmark of our *GW*/BSE method, Figure 3 shows the computed and experimental[20] absorption spectra for three different angular DBC molecules. The corresponding molecules are illustrated inside each graph. The DP, DT, and DBT groups are attached at R3 and R4 positions, while the TES is attached at R1 and R2 positions. The first BSE peaks at 2.45, 2.46, and 2.45 eV for DP-, DT- and DBT-TES-DBC present offsets of 0.04, 0.10, and 0.07 eV, respectively, with respect to the corresponding experimental peaks. On the other hand, the second peaks for DP- and DT-TES-DBC show large offsets of 0.29 and 0.25 eV, respectively, with respect to experiments. For the DBT-TES-DBC, the combination of the second and third BSE peaks (at 2.89 and 3.01 eV) seems to correctly reproduce the experimental peak centered at 3.03 eV. Both experimental and computed data suggest that the substitutions of functional groups at R3 and R4 positions have little influence on the position of the first absorption peak. For the second peaks at higher energies, experimental and computed spectra show red shifts when substituting the DP- with DT- and DBT- functional groups at R3 and R4 positions. In this case, the effect of the functional groups are clearly observed. Despite overestimating the position of the second peak for DP- and DT-DBC molecules, the red shift between them is correctly predicted with an experimental shift of 0.19 eV, while the BSE shift is at 0.22 eV. As already seen in some
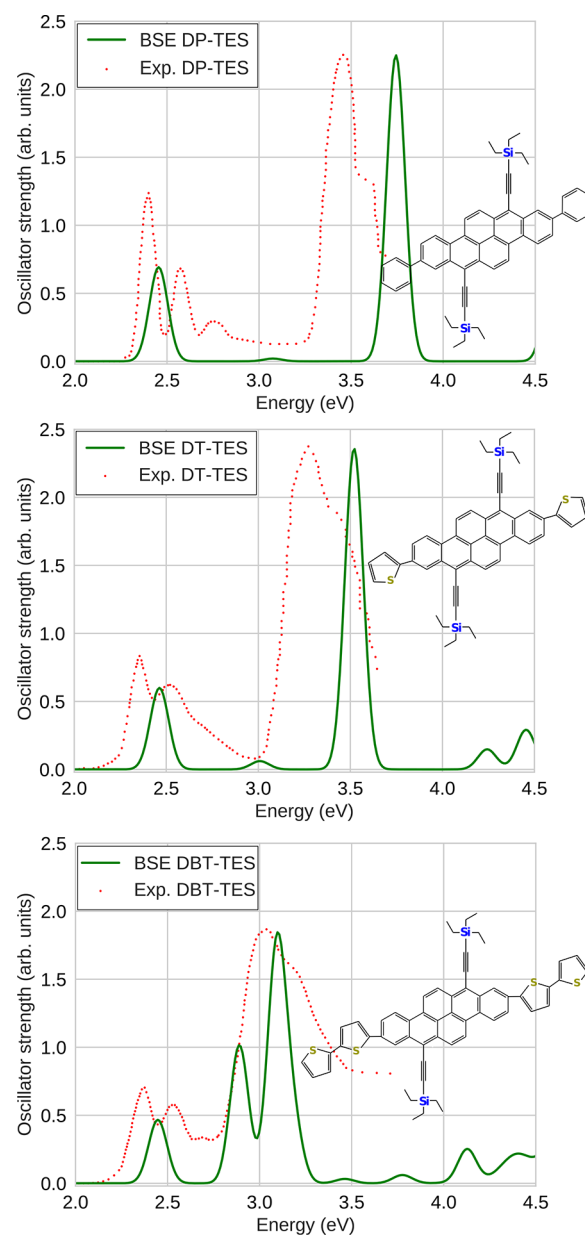
Figure 3. Computed (green) and experimental (red, in solution with $CHCl_3$) absorption spectra for DT-, DP-, and DBT- TES-DBC molecules. The experimental absorption spectra are taken from ref 20.

previous examples, experimental secondary peaks between 2.5 and 2.75 eV are not predicted by the theory.

To summarize the first set of calculations, the *GW*/BSE method allows us to predict the position of the first absorption peaks of a DBC type molecule with an accuracy of ±0.1 eV. However, the offsets between experimental and calculated peak positions can reach up to ±0.3 eV at higher energies. Moreover, in some cases, vibronic secondary peaks are not predicted by the method. One possible explanation of these discrepancies is related to the limits of our simulations which are performed for the gas phase at zero Kelvin so that they do not necessarily reproduce the experimental conditions in which the molecule is surrounded by a solvent at ambient temperature. Despite these limitations, the MBPT seems to correctly reproduce the trend in the shift of the main peaks when substituting functional groups. Finally, the example of the thin film for TIPS-C-DBC suggests that the absorption range of the solid-state material can be
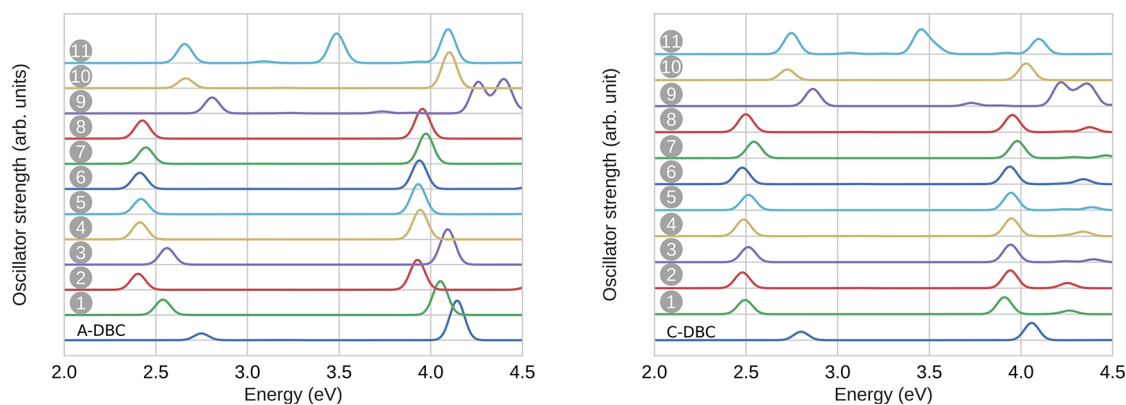
Figure 4. Computed absorption spectra for the angular (left) and compact (right) DBCs with substituents at R1 and R2 positions: the angular and compact DBCs are at the bottom in blue, next from bottom to top, the modified compact DBCs with groups from 1 to 11 (Figure 1c) are plotted.
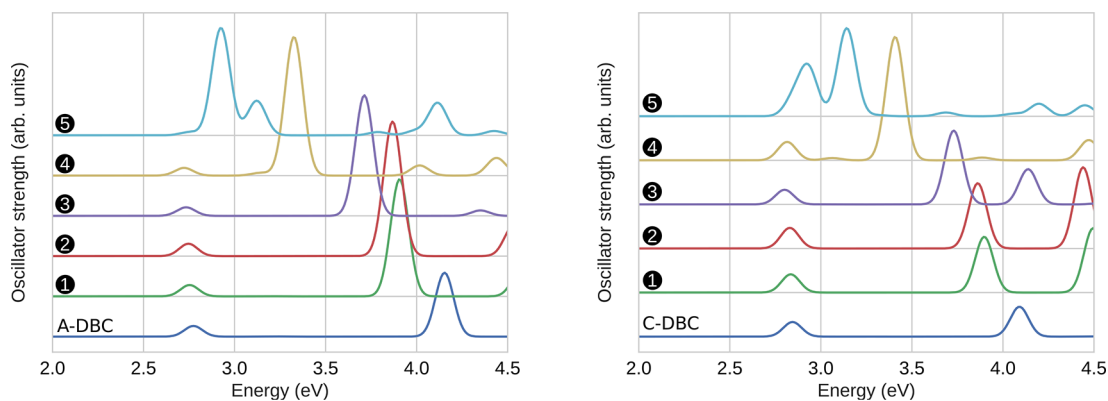
Figure 5. Computed absorption spectra for the angular (left) and compact (rigth) DBCs with substituents at R3 and R4 positions: the angular and compact DBCs are at the bottom in blue, next from bottom to top, the modified DBCs with groups from 1 to 5 (Figure 1d) are plotted.
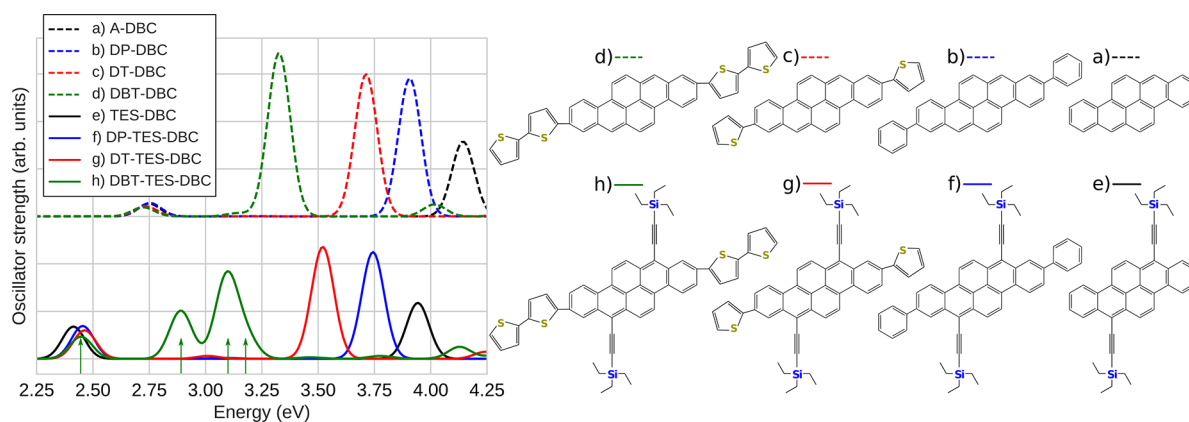
Figure 6. Computed absorption spectra for different angular DBC molecules. For the DBT-TES-DBC, the four absorption peaks (1−4 from left to right) are indicated with green arrows.

extrapolated from the BSE computed absorption spectrum. In the next part, results are presented for newly designed molecules with a more systematic approach.

Predictions. Figures 4 and 5 show the computed absorption spectra for all modified DBCs at R1 and R2 and at R3 and R4 positions, respectively. From a general standpoint, all the functional groups attached at R1 and R2 produce a small decrease in energy for the first exciton and an even smaller decrease for the second exciton. Only two exceptions are observed. First, the triphenyl group (9 in Figures 1c and 4) induces an increase of ~0.1 eV for the first peak and the creation

of a double peak ∼ 0.2 eV higher for the second peak. Second, the 2-cyano-3-(thiophen-2-yl) acrylic acid group (11 in Figures 1c and 4) induces a large red shift of 0.65 eV on the second peak. As for the substitution at R3 and R4 positions illustrated in Figure 5, a red shift of the second peak is observed for all functional groups, while it does not seem to have any influence on the first peak. It is worth noting the effect of the same 2-cyano-3-(thiophen-2-yl) acrylic acid group (5 in Figures 1d and 5), which induces a large red shift (with the creation of a double peak). Finally, the oscillator strength of the second peak is found to be larger for the

a) 1: 2.74 eV (0.26)   b) 1: 2.41 eV (0.68)   2: 3.94 eV (1.18)   c) 1: 2.72 eV (0.20)
2: 4.14 eV (1.57)   2: 3.32 eV (3.44)

d) 1: 2.44 eV (0.46)   2: 2.89 eV (1.01)   3: 3.09 eV (1.73)   4: 3.12 eV (0.43)
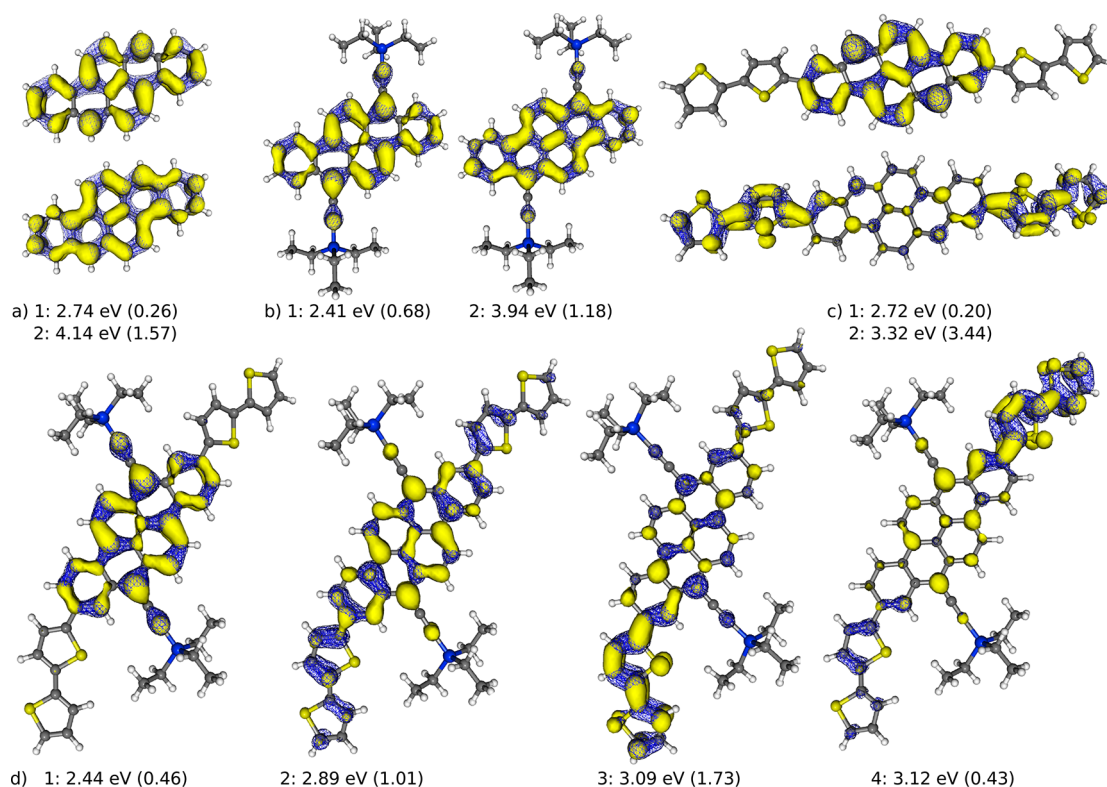
Figure 7. Hole-averaged electron (in yellow) and electron-averaged hole (in wireframed blue) densities of the excitonic states (a) A-DBC, (b) TES-DBC, (c) DBT-DBC, and (d) DBT-TES-DBC. For each exciton, its reference number, its energy level, and, between parentheses, its oscillator strength (in arb. units) are reported below the corresponding densities.

angular DBC compared to the compact DBC, and this observation holds for the modified DBCs.

Figure 6 shows the computed absorption spectra and their illustration for various DBC molecules. Starting from A-DBC, which is illustrated in Figure 6a and adding a di(phenyl), a di(thiophenyl), and a di(bithiophenyl) at R3 and R4 positions, DP- (Figure 6b), DT- (Figure 6c), and DBT-DBC (Figure 6d) are formed, respectively. By adding TES at R1 and R2 positions, the molecules from (a) to (d) in Figure 6 transform into those shown in (e) to (h) in Figure 6. The first absorption peaks for the molecules without TES (dashed lines) are centered at 2.74 eV (±0.01), while the first absorption peaks for the molecules with TES (continuous lines) are centered at 2.44 eV (±0.02). This confirms the trend that functional groups at R3 and R4 have very little influence on the absorption onset. This low-energy transition is a HOMO–LUMO transition with weak overlap between holes and electrons, displaying nodes on the atoms (see Figure 7a), and corresponds to the "ionic" ^1L_a transition with partial charge-transfer character in aromatic hydrocarbons.[46,47] As such, this kind of excitation cannot be stabilized by delocalization with conjugated sidechains. On the other hand, the second peak of A-DBC seems to be red-shifted by the addition of functional groups at R3 and R4 positions (DP-DBC, DT-DBC, and DBT-DBC in Figure 6). The functional groups DP, DT, and DBT, attached at R3 and R4 positions, decrease the energy of the second exciton by 0.24, 0.43, and 0.82 eV, respectively. These red shifts of the second peaks are almost identically reproduced for the molecules with TES (third peak for DBT-TES-DBC) with a red shift of 0.20, 0.42, and 0.84 eV for the DP, DT, and DBT substitutions, respectively. It is worth noting that the addition of two thiophenyl (DBT) produces a red shift exactly twice larger than the one with one thiophenyl (DT).

While the addition of functional groups at R3 and R4 positions has no influence on the first peak, the addition of the TES group at R1 and R2 positions (dashed to continuous lines) produces a constant red shift of 0.3 eV (±0.03 eV). As for the second peaks, the addition of TES also induces a constant red shift of 0.19 eV (±0.03 eV). The shape of the spectrum for DBT-TES-DBC is more complex. First, a new peak appears at 2.89 eV (indicated by a green arrow). Second, a fourth active exciton at 3.12 eV (fourth green arrow) is present but hidden by the third peak centered at 3.09 eV (third green arrow). This fourth BSE peak seems to be in accordance with the small bump at the same energy in the experimental spectrum of DBT-TES-DBC (see Figure 3).

Figure 7 shows the hole-averaged electronic and electron-averaged hole densities (e-h densities) for the excitonic states corresponding to the main absorption peaks of molecules A-DBC, TES-DBC, DBT-DBC, and DBT-TES-DBC (illustrated in Figure 6). The small red shift of 0.33 and 0.20 eV induced by the addition of TES for the first and second peaks, respectively, can be explained by the small modifications of the e-h densities. Compared to A-DBC, the e-h density of TES-DBC stays almost identical on the backbone DBC with only a small delocalization toward the first carbon atom of the TES. This delocalization of the excitonic particle induces the red shift. On the other hand, the addition of the DBT group to the A-DBC (to form DBT-DBC) does not modify the e-h density for the first peak, hence the same excitonic energy in both molecules. The second e-h density of DBT-DBC is completely different from the second e-h density of A-DBC. It is spread all over the molecules with the main part on the DBT functional group allowing for a red shift of 0.82 eV. Finally, the first e-h density of DBT-TES-DBC looks like the first e-h density of TES-DBC, hence the same excitonic energy around 2.4 eV. This confirms that functional groups at R3 and R4

positions do not influence the first peak. The second e-h density of DBT-TES-DBC at 2.89 eV looks like the second one of DBT-DBC, at 3.32 eV, but is more evenly spread over the DBC part. Since the delocalization of the e-h density is more important is this case, the energy will be lower with a red shift of 0.43 eV. The e-h densities for the third and fourth excitons of DBT-TES-DBC look as if they had been obtained by splitting the second exciton of DBT-DBC (at 3.32 eV) with e-h density mainly spread on the DBT group and a little presence on the DBC backbone. As already seen above, the addition of TES at R1 and R2 positions induces a red shift of ~0.20 eV (3.32 to 3.09 eV for the third peak and 3.32 to 3.12 eV for the fourth peak).

Since functional groups at R3 and R4 positions were found to produce a red shift for the second peak of a DBC molecule, newly designed molecules were tested with 1 (DP), 2 (DBT), 3 and 4 added thiophenyls at R3 and R4 positions on a C-DBC. These molecules are illustrated in Figure 8 alongside with their
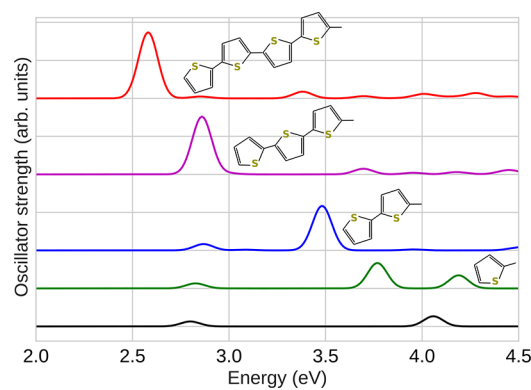
Figure 8. Computed absorption spectra for compact DBC (black curve) and for functionalized compact DBCs with 1 (green), 2 (blue), 3 (violet), and 4 (red) thiophenyl groups attached at R3 and R4 positions.

computed absorption spectrum. A red shift of the second peak of C-DBC is observed and is proportional to the number of added thiophenyls. Figure 9 shows the e-h densities of the first and second excitons for these four molecules and for the C-DBC. Again, the e-h density of the first exciton is not influenced by the functional groups (left column in Figure 9). As for the second exciton (right column in Figure 9), the thiophenyl groups induce a delocalization of the e-h densities and consequently a decrease in energy of the exciton. This red shift also goes alongside with an increase in the oscillator strengths. With 3 and 4 added thiophenyls, the second peaks at 2.85 and 2.58 eV are right in the middle of the visible spectrum (1.65−3.26 eV) and with large oscillator strengths. With such absorption spectra, these newly designed DBCs could potentially improve the efficiency of DBC-based solar cells by collecting a larger part of the solar spectrum. A fine mixing of different modified DBCs could be developed in order to overlap the full solar spectrum and then even further improve efficiencies.

CONCLUSIONS

The *GW*/BSE calculations have been demonstrated to be a precise method to predict the optical gap of DBC molecules. Despite a lower accuracy to describe absorption peaks at higher energies, this method allows us to predict the effect of different functional groups on the optical properties of DBC. The influence of the position where these groups are linked to the DBC backbone has been investigated. In particular, the addition
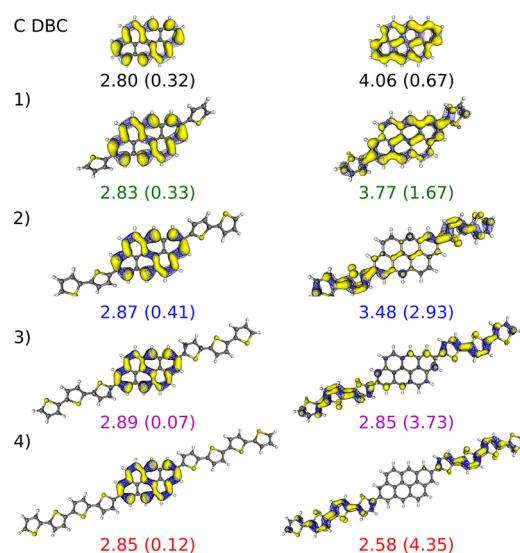
Figure 9. Hole-averaged electronic (in yellow) and electron-averaged hole (in wireframed blue) densities of the excitonic states for the molecules illustrated in Figure 8. Left column: exciton localized on the backbone DBC. Right column: exciton localized on the thiophenyl groups. For each exciton, its energy level and, between parentheses, its oscillator strength (in arb. units) are reported below the corresponding densities.

of thiophenyl groups could be a strategic way to shift high energy absorption peaks to the visible region. These results could pave the way to the creation of new molecules with high absorption in the visible region in order to improve the corresponding efficiencies of future organic solar cells.

AUTHOR INFORMATION

Corresponding Author

*E-mail: gian-marco.rignanese@uclouvain.be. Phone: +32 (0)10 479623. Fax: +32 (0)10 473102.

ORCID

Nicolas Dardenne: 0000-0002-3683-4790
Giuliano Malloci: 0000-0002-5985-257X

Notes

The authors declare no competing financial interest.

REFERENCES

(1) Appleton, A. L.; Brombosz, S. M.; Barlow, S.; Sears, J. S.; Bredas, J.-L.; Marder, S. R.; Bunz, U. H. F. Effects of Electronegative Substitution on the Optical and Electronic Properties of Acenes and Diazaacenes. *Nat. Commun.* **2010**, *1*, 91.

(2) Lucas, B.; Trigaud, T.; Videlot-Ackermann, C. Organic Transistors and Phototransistors Based on Small Molecules. *Polym. Int.* **2012**, *61*, 374−389.

(3) Yang, Y.; da Costa, R. C.; Fuchter, M. J.; Campbell, A. J. Circularly Polarized Light Detection by a Chiral Organic Semiconductor Transistor. *Nat. Photonics* **2013**, *7*, 634−638.

(4) Kotwica, K.; Bujak, P.; Wamil, D.; Pieczonka, A.; Wiosna-Salyga, G.; Gunka, P. A.; Jaroch, T.; Nowakowski, R.; Luszczynska, B.; Witkowska, E.; et al. Structural, Spectroscopic, Electrochemical, and Electroluminescent Properties of Tetraalkoxydinaphthophenazines: New Solution-Processable Nonlinear Azaacenes. *J. Phys. Chem. C* **2015**, *119*, 10700−10708.

(5) Li, J.; Zhang, Q. Linearly Fused Azaacenes: Novel Approaches and New Applications Beyond Field-Effect Transistors (FETs). *ACS Appl. Mater. Interfaces* **2015**, *7*, 28049−28062.

(6) Hoff, J. J.; Zhu, L.; Dong, Y.; Albers, T.; Steel, P. J.; Cui, X.; Wen, Y.; Lebedyeva, I.; Miao, S. Diazapentacene Derivatives: Synthesis, Properties, and Structures. *RSC Adv.* **2016**, *6*, 86824−86828.

(7) Anthony, J. E. Functionalized Acenes and Heteroacenes for Organic Electronics. *Chem. Rev.* **2006**, *106*, 5028−5048.

(8) Burke, K. B.; Shu, Y.; Kemppinen, P.; Singh, B.; Bown, M.; Liaw, I. I.; Williamson, R. M.; Thomsen, L.; Dastoor, P.; Belcher, W.; et al. Single Crystal X-ray, AFM, NEXAFS, and OFET Studies on Angular Polycyclic Aromatic Silyl-Capped 7,14-Bis(ethynyl)Dibenzo[b,def]chrysenes. *Cryst. Growth Des.* **2012**, *12*, 725−731.

(9) Li, M.; Kou, L.; Diao, L.; Zhang, Q.; Li, Z.; Wu, Q.; Lu, W.; Pan, D. Theoretical Study of Acene-Bridged Dyes for Dye-Sensitized Solar Cells. *J. Phys. Chem. A* **2015**, *119*, 3299−3309.

(10) Walker, B.; Kim, C.; Nguyen, T.-Q. Small Molecule Solution-Processed Bulk Heterojunction Solar Cells. *Chem. Mater.* **2011**, *23*, 470−482.

(11) Winzenberg, K. N.; Kemppinen, P.; Fanchini, G.; Bown, M.; Collis, G. E.; Forsyth, C. M.; Hegedus, K.; Singh, T. B.; Watkins, S. E. Dibenzo[b,def]chrysene Derivatives: Solution-Processable Small Molecules that Deliver High Power-Conversion Efficiencies in Bulk Heterojunction Solar Cells. *Chem. Mater.* **2009**, *21*, 5701−5703.

(12) Zhang, L.; Walker, B.; Liu, F.; Colella, N. S.; Mannsfeld, S. C. B.; Watkins, J. J.; Nguyen, T.-Q.; Briseno, A. L. Triisopropylsilylethynyl-Functionalized Dibenzo[def,mno]chrysene: a Solution-Processed Small Molecule for Bulk Heterojunction Solar Cells. *J. Mater. Chem.* **2012**, *22*, 4266−4268.

(13) Chen, H.-Y.; Chao, I. Toward the Rational Design of Functionalized Pentacenes: Reduction of the Impact of Functionalization on the Reorganization Energy. *ChemPhysChem* **2006**, *7*, 2003−2007.

(14) Lobanova Griffith, O.; Gruhn, N. E.; Anthony, J. E.; Purushothaman, B.; Lichtenberger, D. L. Electron Transfer Parameters of Triisopropylsilylethynyl-Substituted Oligoacenes. *J. Phys. Chem. C* **2008**, *112*, 20518−20524.

(15) Feng, X.; Li, Q.; Gu, J.; Cotton, F. A.; Xie, Y.; Schaefer, H. F. Perfluorinated Polycyclic Aromatic Hydrocarbons: Anthracene, Phenanthrene, Pyrene, Tetracene, Chrysene, and Triphenylene. *J. Phys. Chem. A* **2009**, *113*, 887−894.

(16) Sun, H.; Putta, A.; Billion, M. Arene Trifluoromethylation: An Effective Strategy to Obtain Air-Stable n-Type Organic Semiconductors with Tunable Optoelectronic and Electron Transfer Properties. *J. Phys. Chem. A* **2012**, *116*, 8015−8022.

(17) Zhang, L.; Fonari, A.; Zhang, Y.; Zhao, G.; Coropceanu, V.; Hu, W.; Parkin, S.; Brédas, J.-L.; Briseno, A. L. Triisopropylsilylethynyl-Functionalized Graphene-Like Fragment Semiconductors: Synthesis, Crystal Packing, and Density Functional Theory Calculations. *Chem. - Eur. J.* **2013**, *19*, 17907−17916.

(18) Shu, Y.; Collis, G. E.; Dunn, C. J.; Kemppinen, P.; Winzenberg, K. N.; Williamson, R. M.; Bilic, A.; Singh, T. B.; Bown, M.; McNeill, C. R.; et al. The Impact of Tetrahedral Capping Groups and Device Processing Conditions on the Crystal Packing, Thin Film Features and OFET Hole Mobility of 7,14-Bis(ethynyl)Dibenzo[b,def]chrysenes. *J. Mater. Chem. C* **2013**, *1*, 6299−6307.

(19) Geng, Y.; Yi, C.; Bircher, M. P.; Decurtins, S.; Cascella, M.; Grätzel, M.; Liu, S.-X. Anthanthrene Dye-Sensitized Solar Cells: Influence of the Number of Anchoring Groups and Substitution Motif. *RSC Adv.* **2015**, *5*, 98643−98652.

(20) Kim, Y.; Lee, S. B.; Jang, S. H.; An, T. K.; Kim, S. H.; Kim, Y.-H.; Park, C. E. Engineering the Morphologies and Charge Transport Properties of Newly Synthesized Dibenzochrysene-Based Small Molecules by Attaching Various Side Groups. *Dyes Pigm.* **2016**, *130*, 176−182.

(21) Koldemir, U.; Tinkham, J. S.; Johnson, R.; Lim, B.; Yemam, H. A.; Gagnon, K. J.; Parkin, S.; Sellinger, A. Orthogonal 4,10 and 6,12 Substitution of Dibenzo[def,mno]chrysene Polycyclic Aromatic Small Molecules. *J. Mater. Chem. C* **2017**, *5*, 8723−8733.

(22) Cardia, R.; Malloci, G.; Mattoni, A.; Cappellini, G. Effects of TIPS-Functionalization and Perhalogenation on the Electronic, Optical, and Transport Properties of Angular and Compact Dibenzochrysene. *J. Phys. Chem. A* **2014**, *118*, 5170−5177.

(23) Onida, G.; Reining, L.; Rubio, A. Electronic Excitations: Density-Functional versus Many-Body Green's-Function Approaches. *Rev. Mod. Phys.* **2002**, *74*, 601−659.

(24) Kohn, W.; Sham, L. J. Self-Consistent Equations Including Exchange and Correlation Effects. *Phys. Rev.* **1965**, *140*, A1133−1138.

(25) Hohenberg, P.; Kohn, W. Inhomogeneous Electron Gas. *Phys. Rev.* **1964**, *136*, B864−871.

(26) Valiev, M.; Bylaska, E. J.; Govind, N.; Kowalski, K.; Straatsma, T. P.; Van Dam, H. J. J.; Wang, D.; Nieplocha, J.; Apra, E.; Windus, T. L.; et al. NWChem: A Comprehensive and Scalable Open-Source Solution for Large Scale Molecular Simulations. *Comput. Phys. Commun.* **2010**, *181*, 1477−1489.

(27) Becke, A. D. Density-Functional Thermochemistry. III. The Role of Exact Exchange. *J. Chem. Phys.* **1993**, *98*, 5648−5652.

(28) Lee, C.; Yang, W.; Parr, R. G. Development of the Colle-Salvetti Correlation-Energy Formula into a Functional of the Electron Density. *Phys. Rev. B: Condens. Matter Mater. Phys.* **1988**, *37*, 785−789.

(29) Rassolov, V. A.; Ratner, M. A.; Pople, J. A.; Redfern, P. C.; Curtiss, L. A. 6-31G* Basis Set for Third-Row Atoms. *J. Comput. Chem.* **2001**, *22*, 976−984.

(30) Grimme, S. Semiempirical GGA-Type Density Functional Constructed with a Long-Range Dispersion Correction. *J. Comput. Chem.* **2006**, *27*, 1787−1799.

(31) Blase, X.; Attaccalite, C.; Olevano, V. First-Principles *GW* Calculations for Fullerenes, Porphyrins, Phtalocyanine, and other Molecules of Interest for Organic Photovoltaic Applications. *Phys. Rev. B: Condens. Matter Mater. Phys.* **2011**, *83*, 115103.

(32) Blase, X.; Attaccalite, C. Charge-Transfer Excitations in Molecular Donor-Acceptor Complexes within the Many-Body Bethe-Salpeter Approach. *Appl. Phys. Lett.* **2011**, *99*, 171909.

(33) Jacquemin, D.; Duchemin, I.; Blase, X. Benchmarking the Bethe-Salpeter Formalism on a Standard Organic Molecular Set. *J. Chem. Theory Comput.* **2015**, *11*, 3290−3304.

(34) Zhao, Y.; Truhlar, D. G. A New Local Density Functional for Main-Group Thermochemistry, Transition Metal Bonding, Thermochemical Kinetics, and Noncovalent Interactions. *J. Chem. Phys.* **2006**, *125*, 194101.

(35) Papajak, E.; Leverentz, H. R.; Zheng, J.; Truhlar, D. G. Efficient Diffuse Basis Sets: cc-pVxZ+ and maug-cc-pVxZ. *J. Chem. Theory Comput.* **2009**, *5*, 1197−1202.

(36) Duchemin, I.; Deutsch, T.; Blase, X. Short-Range to Long-Range Charge-Transfer Excitations in the Zincbacteriochlorin-Bacteriochlorin Complex: A Bethe-Salpeter Study. *Phys. Rev. Lett.* **2012**, *109*, 167801.

(37) Boulanger, P.; Jacquemin, D.; Duchemin, I.; Blase, X. Fast and Accurate Electronic Excitations in Cyanines with the Many-Body Bethe-Salpeter Approach. *J. Chem. Theory Comput.* **2014**, *10*, 1212−1218.

(38) Marenich, A. V.; Cramer, C. J.; Truhlar, D. G. Universal Solvation Model Based on Solute Electron Density and on a Continuum Model of the Solvent Defined by the Bulk Dielectric Constant and Atomic Surface Tensions. *J. Phys. Chem. B* **2009**, *113*, 6378−6396.

(39) Jones, R. O.; Gunnarsson, O. The Density Functional Formalism, its Applications and Prospects. *Rev. Mod. Phys.* **1989**, *61*, 689−746.

(40) Shah, B. K.; Neckers, D. C.; Shi, J.; Forsythe, E. W.; Morton, D. Photophysical Properties of Anthanthrene-Based Tunable Blue Emitters. *J. Phys. Chem. A* **2005**, *109*, 7677−7681.

(41) Reichardt, C. *Solvents and Solvent Effects in Organic Chemistry*; Wiley-VCH Verlag GmbH & Co. KGaA: Weinheim, Germany, 2002; pp 329−388.

(42) Cardia, R.; Malloci, G.; Rignanese, G.-M.; Blase, X.; Molteni, E.; Cappellini, G. Electronic and Optical Properties of Hexathiapentacene in the Gas and Crystal Phases. *Phys. Rev. B: Condens. Matter Mater. Phys.* **2016**, *93*, 235132.

(43) The model system with an explicit first solvation shell was generated as follows. First, we placed 20 CH_2Cl_2 molecules at random around the C-DBC within a distance of 5 Å. Finally, all the atomic positions were relaxed first using the MMFF94 force field and, then, using DFT (adopting the same parameters as for the isolated molecules).

(44) Li, J.; D'Avino, G.; Duchemin, I.; Beljonne, D.; Blase, X. Combining the Many-Body *GW* Formalism with Classical Polarizable Models: Insights on the Electronic Structure of Molecular Solids. *J. Phys. Chem. Lett.* **2016**, *7*, 2814−2820.

(45) Duchemin, I.; Jacquemin, D.; Blase, X. Combining the GW Formalism with the Polarizable Continuum Model: A State-Specific Non-Equilibrium Approach. *J. Chem. Phys.* **2016**, *144*, 164106.

(46) Rangel, T.; Hamed, S. M.; Bruneval, F.; Neaton, J. B. An assessment of low-lying excitation energies and triplet instabilities of organic molecules with an ab initio Bethe-Salpeter equation approach and the Tamm-Dancoff approximation. *J. Chem. Phys.* **2017**, *146*, 194108.

(47) Platt, J. R. Classification of Spectra of Cata-Condensed Hydrocarbons. *J. Chem. Phys.* **1949**, *17*, 484−495.